Studies on structural and ionic transport in biopolymer electrolytes based on alginate-LiBr

A. F. Fuzlin [1] · Y. Nagao [2] · I. I. Misnon [1,3] · A. S. Samsudin [1]

Abstract

The development of solid biopolymer electrolytes (SBEs) system based on alginate doped with LiBr was successfully prepared via solution casting. The structural and ionic conduction of SBEs were conducted to correlate the effect of LiBr in alginate by means of Fourier transform infrared (FTIR) spectroscopy, X-ray diffraction (XRD), scanning electron microscope (SEM), thermogravimetric analysis (TGA), differential scanning calorimetry (DSC), and impedance spectroscopy. From the infrared study, SBEs exhibited the occurrence of complexation between lithium-ion and carboxylate ion (COO^-) of alginate through the peak intensity and wavenumber shift. The alginate doped with 15 wt.% LiBr achieved the highest ionic conductivity of 7.46×10^{-5} S/cm at ambient temperature, suggesting its good conduction stability as well as amorphous phase. The IR-deconvolution approach revealed that the ionic conductivity of SBEs system is influenced by both the ionic mobility and diffusion coefficient of transport properties. Based on LSV analysis, it's implies that the present SBEs have the potentiality to be applied in electrochemical devices.

Keywords Biopolymer material · Ionic conductivity · Thermal stability · Ionic transports

Introduction

The rising interest in polymer electrolytes (PEs) is primarily due to its potential applications in various solid-state electrochemical devices. The PEs have demonstrated desirable qualities, for instance, physical flexibility, dimensional stability, long life span, and electrochemical stability, among others [1, 2]. Owing to the aforesaid qualities, it exhibits itself as a promising alternative as electrolyte cum separator in energy devices, such as fuel cell, solar cell, batteries, and electric double-layer capacitors. Many works have been carried out that is devoted to exploring the variety of polymer materials as well as techniques in order to yield good conduction properties of PEs. In general, a polymer can be divided into two types: (1) synthetic polymer and (2) natural polymer. A number of works have been reported on the use of poly (methylmethacrylate) (PMMA) [3], poly (ethylene oxide) (PEO) [4], poly (vinyl chloride) (PVC) [5], and poly (acrylonitrile) (PAN) [6] in the development of PEs. However, it is worth noting that this synthetic polymer is mainly produced from non-renewable resources that, in turn, may affect the environment, particularly with regard to its waste disposal.

In order to overcome such drawbacks, natural polymer from renewable resources has been widely explored as alternative for the development of PEs. Natural polymers or biopolymers have shown a promising substitute for synthetic counterparts, as it presents several advantages such as low cost, non-toxic, abundant availability in nature, and environmental and human body compatibility [7]. Green and eco-friendly SBEs membranes, obtained from biopolymers, have also been investigated over the last two decades [8]. Among investigated are the different polysaccharides-cellulose [9], chitosan [10], dextran [11], gelatin [12], or DNA-based PEs [13]. Such natural polymers have an ability to solvate the ionic dopant or/and produce free delocalized ions due to the interaction between the lone pair of the heteroatom such as oxygen or nitrogen with ionic dopant [14]. Such interaction is noteworthy for the enhancement of conduction properties in the PEs.

✉ A. S. Samsudin
ahmadsalihin@ump.edu.my

1   Ionic Materials Team, Faculty of Industrial Sciences & Technology, Universiti Malaysia Pahang, 26300 Kuantan, Pahang, Malaysia

2   School of Materials Science, Japan Advanced Institute of Science and Technology, 1-1 Asahidai, Nomi, Ishikawa 923-1292, Japan

3   Nanostructured Renewable Energy Materials Laboratory, Faculty of Industrial Sciences & Technology, Universiti Malaysia Pahang, 26300 Kuantan, Pahang, Malaysia

Alginate is a promising candidate for natural low-cost bio-polymer, which can act as a polymer matrix for ionic conduction. Alginate is a brown alga, bioactive anionic polysaccharides composed of (1–4)-linked β-d-mannuronate and (1–4)-linked α-l-guluronate residues which generally have been used in packaging, biomedical fields, and food and textile industries [15–17]. Alginate is an anionic polymer (COO⁻) that is suitable for coordination formation with an ionic dopant and enhances the SBEs conduction properties. The typical procedure for obtaining good SBEs conduction properties is by using alkali metal salts (including lithium salts). The development of lithium ion–based SBEs has drawn considerable attention due to their stability in energy storage applications [18, 19].

Therefore, the aim of this paper is to prepare SBEs based on alginate host and lithium bromide (LiBr) dopant. The alginate-LiBr-based SBEs were characterized for structural, thermal, and conduction properties by using FTIR, XRD, SEM, TGA, DSC, and EIS, respectively. Besides, the ionic transport properties were analyzed using IR-deconvolution method and presented new insights on the conduction behavior of the present SBEs system.

Experimental method

Sample preparation

The SBEs film was prepared using a solution casting technique utilizing alginate (Shaanxi Orient Co. with M.W. ~ 40,000) as a polymer host and LiBr (Sigma-Aldrich with M.W. 86.85 g mol⁻¹) as a dopant. Firstly, 2 g of alginate was dissolved in distilled water (solvent) and followed by the addition of LiBr (between the range of 5 to 25 wt.%). The mixture was continuously stirred at room temperature until a homogenous solution was obtained. The solution was poured into Petri dishes and dried in an oven at 60 °C for 24 h until a solid film was attained. In order to prevent the solvent from being trapped in the SBEs film, the film was further dried in vacuum desiccators filled with silica gel for a period of a month. The sample preparation scheme, physical appearance, and abbreviation (different composition) for the alginate-LiBr system are illustrated in Fig. 1.

Characterization

Fourier transform infrared spectroscopy

The FTIR analysis was conducted using Perkin Elmer Spectrum One equipped with attenuated total reflection (ATR) to investigate the interaction in alginate-LiBr SBEs system. The sample was placed on ATR holder equipped with Ge crystal, and IR light was passed through the sample within

the wavenumber from range 4000 to 700 cm⁻¹ with a resolution of 2 cm⁻¹.

X-ray diffraction

Rigaku MiniFlex II X-ray diffractometer was used to characterize the crystal structure of alginate-LiBr SBEs system. The sample was placed onto a sample holder and scanned with a speed of 1.0 s and step size of 0.02° at 2θ = 5 to 80° using Cu $K\alpha$ radiation (λ = 0.154 nm).

Scanning electron microscope

The surface morphological analysis was investigated using FEI quanta 450 scanning electron microscope (SEM) with an accelerating voltage of 10 kV. The prepared samples of SBEs were coated with a thin layer of platinum using Auto Fine Coaters JFC-1600 to prevent electrostatic charging on the electrolytes and reduce thermal damage. SEM characterization was carried out at × 2000 magnification by using Everhart Thornley Detector (ETD).

Thermogravimetric analysis

The thermal properties of SBEs sample were performed using TG-DTA2010SA (NETZSCH, Japan). The measurements were carried out in a nitrogen gas atmosphere at a flow rate of 100 mL min⁻¹. The samples from different composition were heated from 30 to 550 °C at a heating rate of 10 °C min⁻¹, and the mass of each sample is ~ 3 mg.

Differential scanning calorimetry

The thermal properties of the prepared SBEs were determined using a NETZSCH DSC 214 Polyma model. The prepared samples were analyzed at a heating rate of 30 °C min⁻¹ in the temperature range of 30 to 300 °C in a nitrogen atmosphere (flow rate of 62 mL min⁻¹).

Electrical impedance spectroscopy

The ionic conductivity of SBEs films was analyzed using HIOKI 3532-50 LCR Hi-TESTER at a fixed constant voltage level of 0.1 V and a frequency range of 50 Hz to 1 MHz. The SBEs sample was placed between two stainless steel electrode and tested at a temperature range from 303 to 343 K. The determination of ionic conduction for SBEs sample was operated in convention oven in order to control environment humidity effect. From the EIS parameter, the imaginary impedance (Zi) versus real impedance (Zr) of Cole-Cole plot and the bulk resistance (Rb) of SBEs sample were identified. Based on the R_b value, the ionic conductivity, σ, was determined using the following equation:

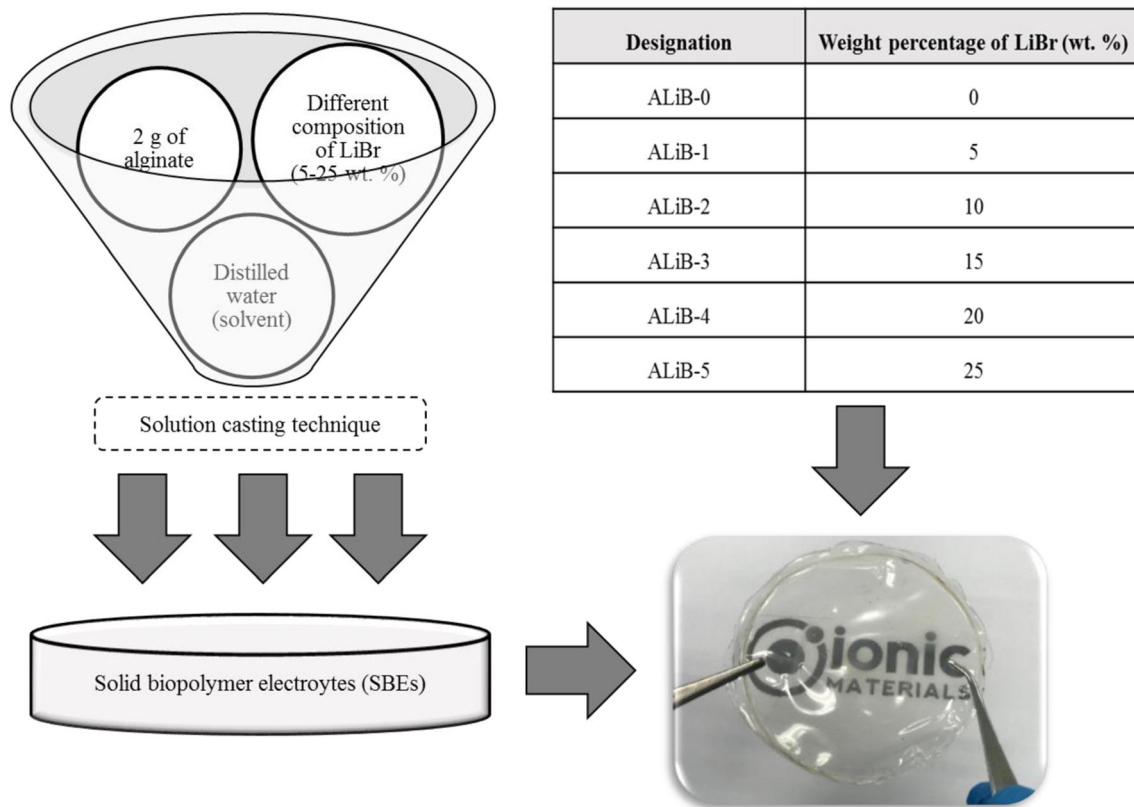| Designation	Weight percentage of LiBr (wt. %)
ALiB-0	0
ALiB-1	5
ALiB-2	10
ALiB-3	15
ALiB-4	20
ALiB-5	25

Fig. 1 Sample preparation scheme, physical appearance, and abbreviation of alginate-LiBr SBEs system

$$\sigma = \frac{t}{R_b A} \quad (1)$$

where t and A are sample thickness and cross-sectional area of the SBEs film, respectively. All the EIS measurements were repeated three times for each sample, and the average value was calculated.

Transport properties

The FTIR deconvolution approach is used in order to determine the transport properties of SBEs system, which retrieved using OriginLab 8.0 software. The absorbance peaks were fitted to a straight baseline and the area under the peaks was determined. The free ion percentage (%) was calculated using the following equation,

$$\text{Percentage of free ions } (\%) = \left[\frac{A_f}{A_f + A_c}\right] \times 100\% \quad (2)$$

where A_f is the area under the peak representing the region of the free ions and A_c is the total area under the peak representing the contact ions' region. The number of mobile ions (η), ionic mobility (μ), and diffusion coefficient (D) of the SBEs system were measured using the following equations,

$$\eta = \left[\frac{MN_A}{V_{\text{Total}}}\right] \times \text{free ions } (\%) \quad (3)$$

$$\mu = \frac{\sigma}{\eta e} \quad (4)$$

$$D = \frac{KT\mu}{e} \quad (5)$$

where M is the LiBr mole number, N_A is Avogadro's number, V_{Total} is the total volume of the alginate-LiBr SBEs, e is the electron charge, K is the Boltzmann constant, and T is the absolute temperature.

Voltammetry measurement

Linear sweep voltammetry (LSV) measurements were analyzed using PGSTAT M101 potentiostat with FRA32M module (Metrohm Autolab B.V., the Netherlands). The LSV was used to study the electrochemical stability window of SBEs at ambient temperature. LSV measurements were performed at a scan rate of 5 mV s^{-1} with a range of voltage from 0 to 2 V. The configuration of sample and electrode is similar to what has been reported from the literature where the stainless steel (SS) electrode was used as the reference, working and counter electrodes [20].

Result and discussion

FTIR spectroscopy analysis

The FTIR spectra of pure alginate (ALiB-0) and LiBr are shown in Fig. 2. The peaks at 1045, 1438, 1618, 2403, and 3415 cm^{-1} of ALiB-0 correspond to glycoside bond (C–O–C), symmetric stretching of COO$^-$, antisymmetric stretching of COO$^-$, polymer backbone structure of stretching CH$_2$, and O–H stretching, respectively [21–25]. The peaks correspond to C–O–C and COO$^-$ of alginate are expected to have an interaction in the event that any ionic dopant incorporated in the alginate polymer. This interaction transpires as the alginate polymer contains a strong anion absorption as reported by literature [26, 27]. A sharp absorption peak at 3356 and 1612 cm^{-1} on the LiBr sample was suggested to correspond with the Li$^+$ moiety of the LiBr [28–30]. The inset figure in Fig. 2 shows the optimized molecular structure of alginate which was retrieved from the density functional theory (DFT) based on Dmol3 modules (Material Studio 2017), respectively.

The highlighted wavenumbers that are thought to be the complexation between alginate and LiBr to transpire are presented in Fig. 3. The complexation can be observed by the changes in the absorption peaks (IR wavenumber) in SBEs system.

Based on Fig. 3(a), the C–O–C vibrational stretching band at 1045 cm^{-1} [31] was shifted to a lower wavenumber (1028 cm^{-1}) after the addition of LiBr to ALiB-3. This shift suggests the ion-induced dipole interactions ensued upon the inclusion of lithium salt. In addition, the changes of the peak were affected by the attraction of ionic dopant towards alginate lone pair electrons [32, 33]. Due to the presence of a highly electronegative atom, oxygen atom from the C–O–C
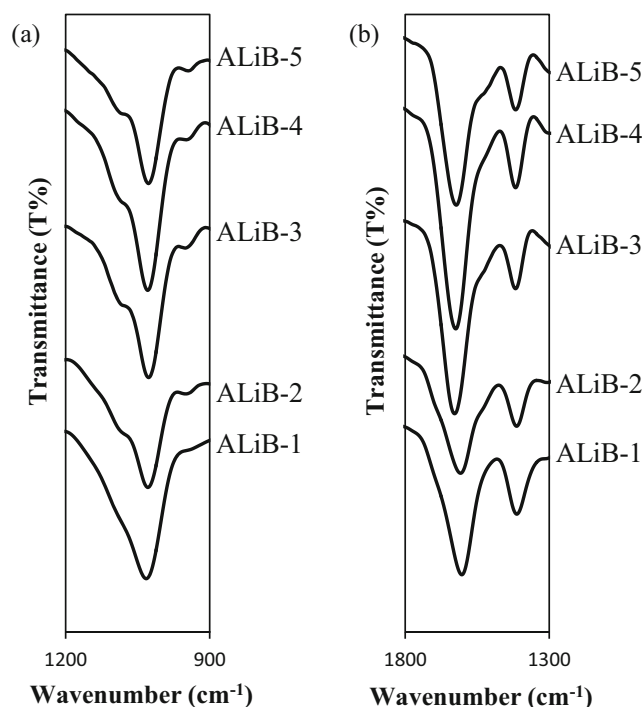
Fig. 3 FTIR spectra of alginate-LiBr SBEs system between range (a) 900 to 1200 cm^{-1} and (b) 1300 to 1800 cm^{-1}

group, the electron pair was donated to the Li$^+$ and, hence, forming the coordinated Li-Br bonding [34].

Figure 3(b) shows the characteristic peak of ALiB-0 at 1438 cm^{-1} and 1618 cm^{-1} that corresponds to both symmetric and asymmetric of the COO$^-$,, and the peak was shifted to a lower and a higher wavenumber value at 1417 cm^{-1} and 1629 cm^{-1} upon the addition of LiBr to ALiB-3. It is expected that dissociation of Li$^+$ cation from LiBr promotes the interaction with the negatively charged lone electron pairs (coordinating site) of COO$^-$ anion in alginate through Coulombic

Fig. 2 FTIR spectra of (a) pure alginate (ALiB-0) and (b) LiBr
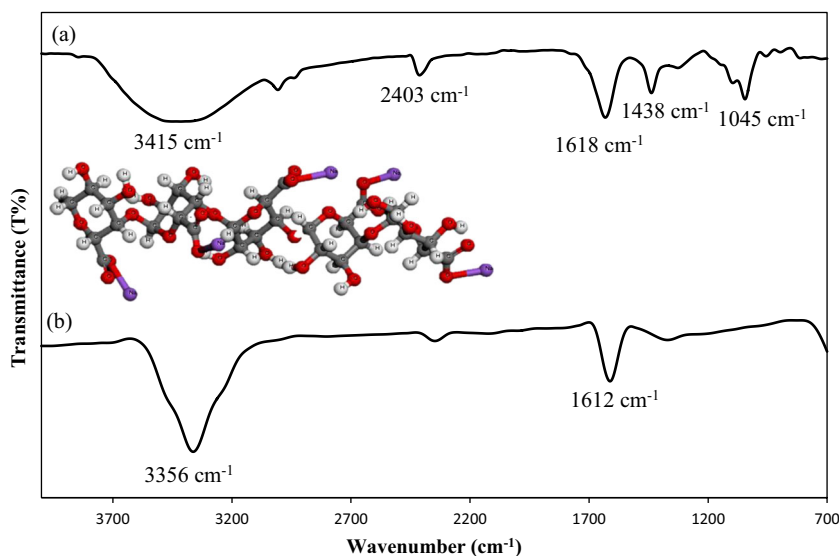
attraction force [35]. This electrostatic attraction is presumed to affect the amorphousness and ionic conductivity of SBEs [36, 37]. Furthermore, upon addition of ionic dopant to ALiB-5, the vibrational bands shifted back to a lower value at 1623 cm^{-1} for asymmetric COO$^-$ and remain unchanged for symmetric COO$^-$ at 1417 cm^{-1}. The changes can be explained by dopant aggregation at higher loading (percolation threshold). It could also lead to the recombination of Li$^+$ with Br$^-$ to form neutral ion pair and thus affects the transport properties and ionic conductivity [38].
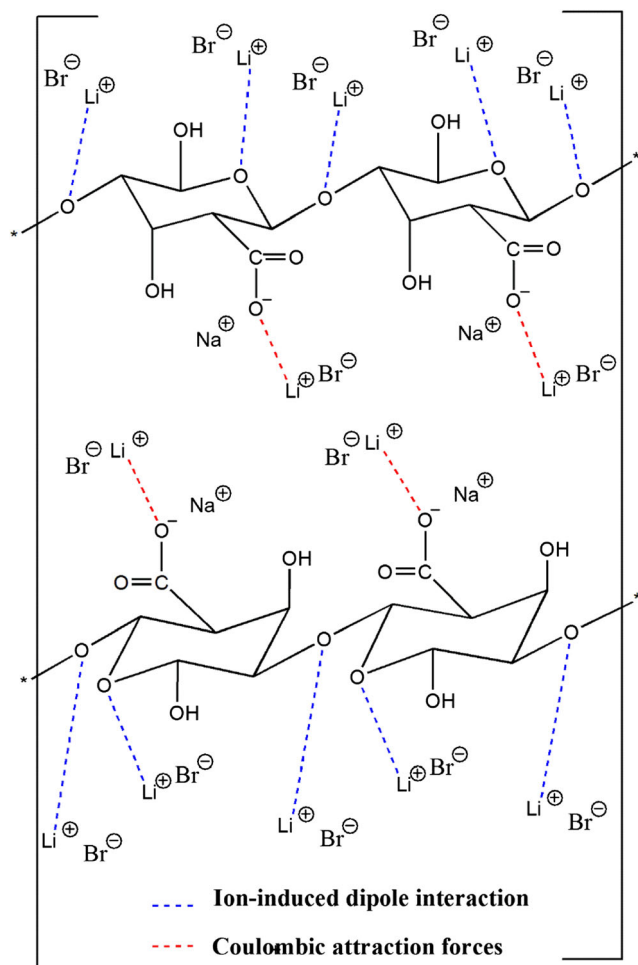
From the findings, it is believed that there is a strong contribution of the coordination interaction of Li$^+$ to the (C–O–C and COO$^-$) between alginate and LiBr and evident that the conduction mechanism is expected to occur as presented in Scheme 1.

X-ray diffraction analysis

Figure 4 depicts the X-ray diffractograms of various SBEs samples. The ALiB-0 has two principal diffraction peaks at $2\theta = 22.12$ and $34.63°$, which indicate two different

Scheme 1 Schematic diagram of alginate interaction with Li$^+$ of LiBr

amorphous regions as reported by other works [39, 40]. As stated by Zhang et al. [41], the pure alginate showed two broad, amorphous peaks attributed to polysaccharide structure. However, a small crystallite peak at 13.84° for ALiB-0 is observed, which may correspond to the alginate characteristic that is similarly reported by other researchers [42, 43].

The reduction of the XRD peak intensity (becoming more amorphous) is observed when LiBr was added in the alginate SBEs. As reported by Hodge et al. [44], the amorphous nature of the polymer matrix can be established by a correlation between the height of the peak intensity and degree of crystallinity. The disappearance of crystallite peak at 13.84° upon addition of LiBr suggests that there is a dissociation of Li$^+$ from Li-Br and formed a coordinating bond with biopolymer matrix as supported by FTIR analysis [45]. The phenomenon affects on energy barrier decrement to the segmental motion of the present SBEs, thus accelerating and inducing Li$^+$ ions to have higher ionic conductivity [46]. Correa et al. reported that the changes of amorphousness in polymer electrolytes would affect the ionic conductivity and conduction properties [47].

Morphological analysis

Figure 5 depicts the surface morphology of SBEs at ambient temperature. From Fig. 5(a), the pure alginate showed a homogeneous, smooth morphology without cracks or pores, indicating a solid structure formation [48]. Upon addition of LiBr, the ALiB-1 microstructure in Fig. 5(b) displayed the rough surface properties which indicates that the samples are homogeneous with amorphous nature. Due to the complete dissolution of salt in the polymer matrix, the enhancement of segmental motion takes place in the SBEs. Such motion produces empty spaces, which enables a more effortless ion flow in the material with electric field presence, and it is expected to increase the ionic conductivity [49]. As shown in Fig. 5(c), the SEM image of ALiB-3 revealed the homogeneity surface without any phase separation that could be due to the ion set-ups in the present SBEs, which enhances the ion transportation, thus establishing the amorphousness of the sample [50].

The dispersion of nanoparticles at the higher composition of LiBr (ALiB-5) was demonstrated to be not uniform, and some agglomeration was observed (Fig. 5(d)). This result is in parallel with the findings of Salman et al., which reported notable aggregation at a higher composition of lithium tetrafluoroborate (LiBF$_4$) in the biopolymer matrix [51]. Excessive LiBr disables the ion interaction with alginate and promotes ion recombination (re-crystallization) [52]. This phenomenon reflects the reduction in the thermal stability and transport properties that in turn reduces the ionic conductivity.
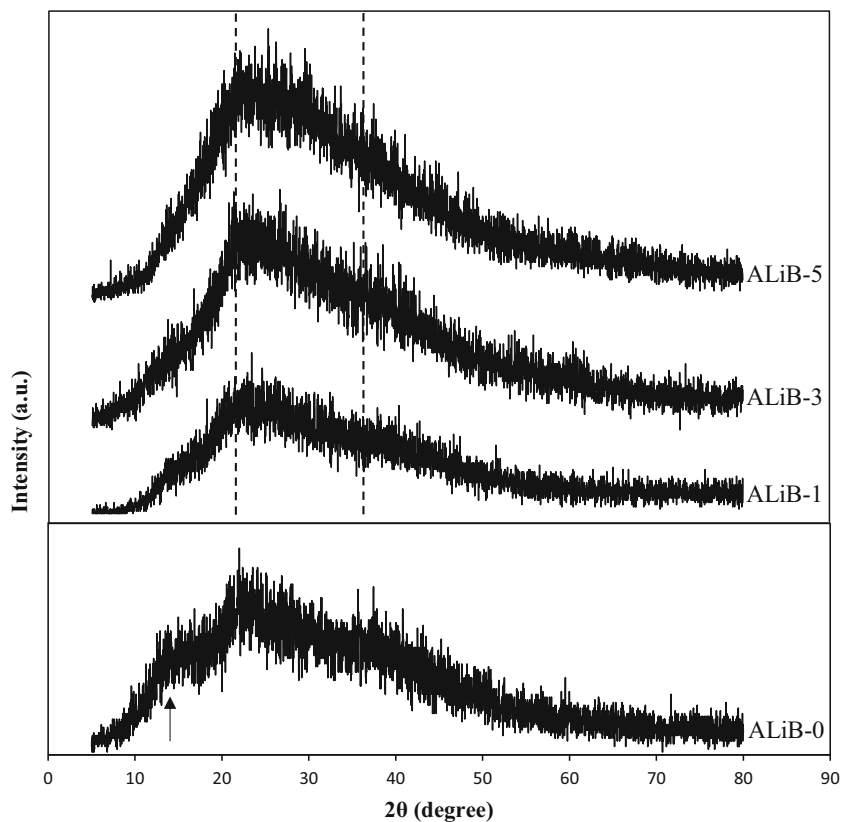
Thermogravimetric analysis

Figure 6 shows the thermogravimetry profiles of SBEs upon heating at a temperature range of 30 to 550 °C under N_2

atmosphere. The thermal degradation process of SBEs was studied by observing sample mass loss as a function of time or temperature. The thermal degradation of pure alginate (ALiB-0) exhibit three-stage degradation process. The initial

Fig. 5 Surface micrographs for (a) ALiB-0, (b) ALiB-1, (c) ALiB-3, and (d) ALiB-5 of alginate-LiBr SBEs system
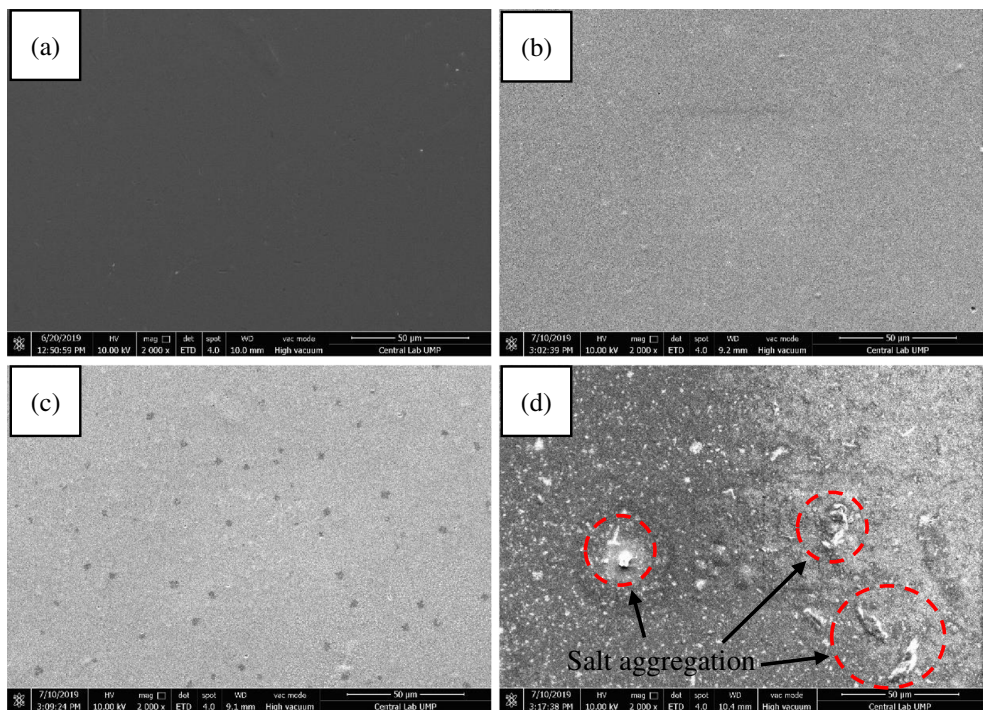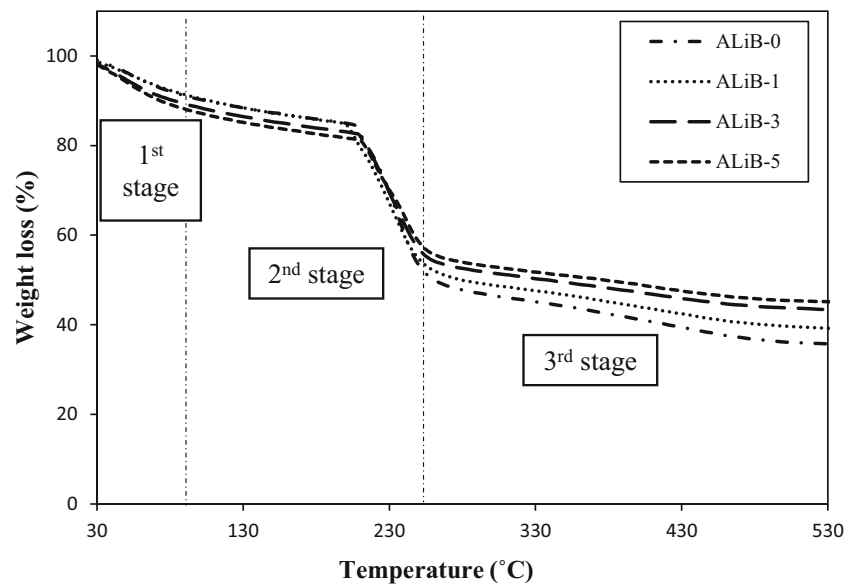
Fig. 6 Thermogram of alginate-LiBr in SBEs system

degradation is due to water loss and decomposition, and the final degradation is due to ring dehydration, cleavage of glycosidic bonds, and decarboxylation of alginate [53, 54].

Three distinct degradation stages were observed for SBEs system and were tabulated in Table 1. The first degradation in SBEs system from room temperature to ∼ 100 °C describes the losses of moisture in biopolymer complexes [55, 56]. According to Kadir and Hamsan (2018), the water weight loss at initial step is due to the hygroscopic nature of polymer [11]. Based on Fig. 6, the second stage decomposition (up to 260 °C) was contributed to the loss of the carboxylate anion group (COO⁻) from the biopolymer backbone [57]. It can be seen that ALiB-0 showed a sudden weight loss of ∼ 33% (decompose stage) with the decompose temperature at 255.89 °C. As reported by Swamy et al. [58], carboxylate groups in the biopolymer backbone of alginate undergo decarboxylation (degradation) in the range of 219 to 261 °C. However, thermogram of ALiB-3 depicts decomposed temperature at 259.71 °C with lower weight loss of ∼ 28% at similar decompose stage compared with ALiB-0. It is shown from the present investigation that the addition of LiBr improved both heat resistivity and thermal stability of SBE complexes. Moreover, the greater amorphous phase as revealed by XRD analysis was due to the increment of the decompose temperature upon the addition of LiBr. This increase in temperature reduces the

energy barrier and causes segmental motion of the polymer electrolytes and, thus, leads to the possible ionic conductivity increment. A similar finding has been reported by Mary et al. [59] for the system based on K-carrageenan complexed with lithium bromide where the amorphous structure of polymer electrolytes would create adequate pathways that increases the thermal stability and ionic mobility and thus improves the conductivity values.

For the third stage (above ∼ 260 °C), a small weight loss was observed with ∼ 12% for ALiB-3. According to Huq et al. (2012), the degradation and charring of the remaining carbon ash from alginate complexes took place when the temperature exceeds ∼ 500 °C [60]. The increment of temperature above 500 °C (prolong heating) resulted in the carbonization of polymer backbone into ash formation [61].

Differential scanning calorimetry analysis

The DSC was used to characterize the thermal properties of complex system in order to further understand the interaction between alginate and LiBr [62]. Figure 7 displays DSC thermograms obtained from the alginate SBEs system. Generally, the glass transition temperatures (T_g) depend upon intermolecular interactions, the molecular weight, the chain flexibility, and branching and cross-linking density [63]. The T_g was measured at the midpoint of each transition, and this method has been reported in the literature [64, 65]. According to Mary et al. [59] and Unnisa et al. [66], the T_g taking place at a range of temperature where its midpoint is accompanied with a maximum shift of heat flow or step-like transition which is considered the mean value of the distribution. The observed T_g for SBEs system is depicted by arrows as shown in the Fig. 7. Figure 7(a) depicted that no T_g was recorded for pure alginate. The pure alginate displayed the endothermic peak, Endo$_{peak}$ at

Table 1 Thermal properties of alginate-LiBr in SBEs system

Sample	Decomposed temperature (°C)	Weight loss (Δ %)
ALiB-0	255.89	32.99
ALiB-1	254.74	31.15
ALiB-3	259.71	28.14
ALiB-5	254.11	24.16

Fig. 7 DSC thermograms of (a) ALiB-0, (b) ALiB-1, (c) ALiB-3, and (d) ALiB-5 SBEs system
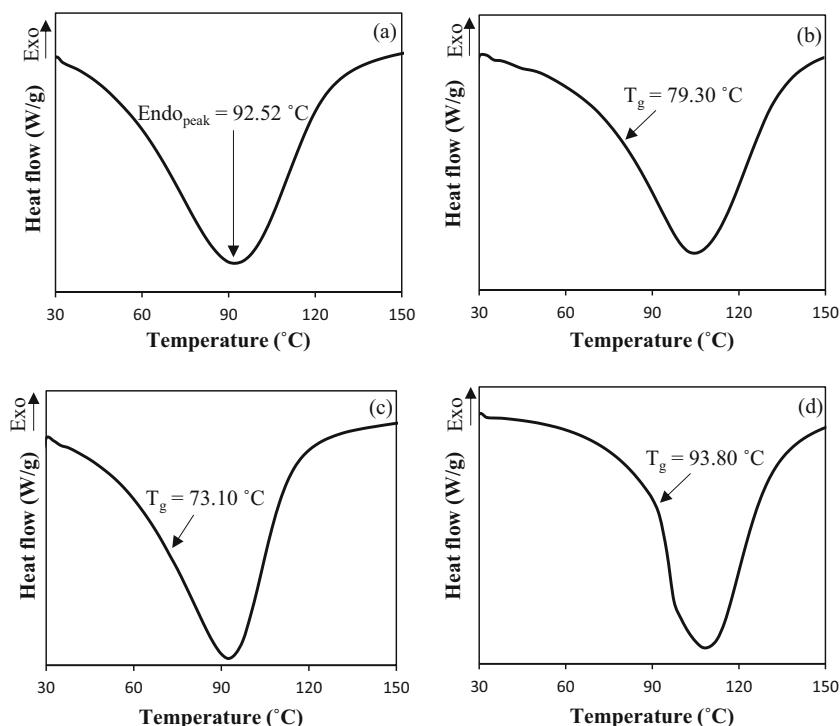
71.70 °C. According to Rezvanian et al. [67], the endotherm is related to the elimination of free water and dehydration of the cross-linked polymer matrix (alginate-sodium cation).

In the SBEs system, a single T_g value was clearly observed with the incorporation of 5 wt.% LiBr (ALiB-1) with the T_g value at 79.30 °C. This T_g is attributed by the formation of coordination between the oxygen atom of polymer matrix chain segments and Li$^+$ from LiBr, which forms the complexation [28]. Notably, the addition of LiBr until 15 wt.% (ALiB-3) affects the T_g value, which is shifted to a lower temperature, thus aiding in the softening of the polymer chain backbone. The decrease in T_g indicates an increment in the flexibility of polymer chains; hence, ALiB-3 is expected to achieve the highest ionic conductivity [26]. Further increase in the composition of LiBr above 15 wt.% leads to the increment of the T_g value. This can be attributed to the formation of ion aggregates in the polymer matrix, which reduced the flexibility of the polymer chain; therefore, Li$^+$ may no longer act as transient cross-linkers [11]. A similar trend has been observed by Arockia Mary (2019) for the system based on k-carrageenan complexed with LiBr where the cross-linkage bonds block the rotation of polymer segments, leading to the hardening of polymer chains and hence intensifying the energy barrier to the segmental movement [59].
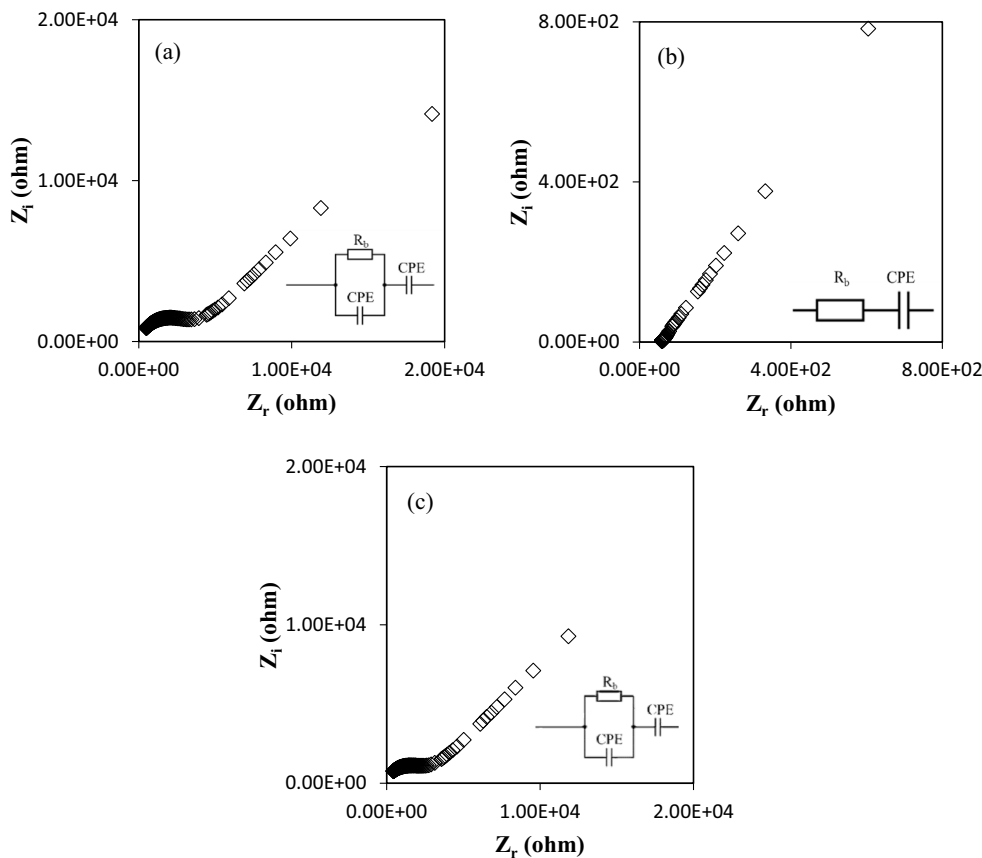
Ionic conductivity analysis

Figure 8 depicts the Cole-Cole plot of various samples' alginate-LiBr-based SBEs at ambient temperature. In the present work, the Cole-Cole plot consists of two different patterns,

i.e., (1) semicircle and a tilted spike and (2) only a tilted spike. Both patterns can be fitted and explained with electrical equivalent circuits, as shown in the inset of Fig. 8. It is apparent that ALiB-1 and ALiB-5 illustrated a combination of an incomplete semicircle and an inclined spike, which corresponds to the ion conduction characteristics with the blocking electrode effect in SBEs [68]. The semicircle can be represented by a parallel combination of bulk resistance (R_b) and constant phase element (CPE) with another CPE in series due to tilted spike, which confirms the semiconducting behavior as reported by other researchers [69, 70]. In the semiconducting materials, the CPE or bulk capacitance behave like "leaky capacitor," in which it functions as a compensator for the inhomogeneity in the SBEs system [71]. Since stainless steel is used as the electrode, the high-frequency semicircle may be associated to the ionic conduction process in the bulk of the SBEs, and the low-frequency spike is attributed by the electrodes blocking effect [72]. On the other hand, ALiB-3 show a full inclined spike with the disappearance of the semicircle and this could lead to ionic conductivity improvement where only the resistive elements prevail in the present SBEs [73]. The Cole-Cole plot for ALiB-3 can be fitted with a resistor connected in series with CPE, and this behavior has also been observed by other works [74, 75]. Figure 9 (inset) shows the R_b value for each composition of alginate-LiBr SBEs system.

From the Cole-Cole plot, the value of R_b was determined (tabulated as inset figure in Fig. 9) and the ionic conductivity of SBEs system was calculated using Eq. 2. Figure 9 shows the ionic conductivity values of alginate doped with different contents of LiBr at ambient temperature. The ionic

Fig. 8 Cole-Cole plot for sample (a) ALiB-1, (b) ALiB-3, and (c) ALiB-5 of alginate-LiBr in SBEs system

conductivity increased from 4.67×10^{-7} S cm^{-1} for ALiB-0 (from previous study) [76] to optimum value at 7.46×10^{-5} S cm^{-1} (sample ALiB-3). The enhancement of ionic conductivity could be attributed to the increment of transport properties, which initiate the Li$^+$ ion transportation in biopolymer segments [77]. Furthermore, the ionic conductivity increment was found to be aligned with the morphological and thermal stability analyses as previously discussed where it creates more space in the biopolymer matrix which reflects

the migration of Li$^+$ to the coordinating site COO$^-$ or C–O–C with lesser of blocking pathway [78, 79]. It shows that beyond the optimum ionic conductivity value of sample ALiB-3, the ionic conductivity started to decrease. This might occur due to the formation of ion aggregation as revealed by XRD and SEM analysis which leads to a decrease in the mobility of ions [45, 80].

Figure 10 depicts the log conductivity versus 1000/T for various sample of alginate-LiBr SBEs system at a temperature

Fig. 9 Ionic conductivity and activation energy of alginate-LiBr SBEs system at ambient temperature. Inset table shows bulk resistance, ionic conductivity, and activation energy of alginate-LiBr in SBEs system
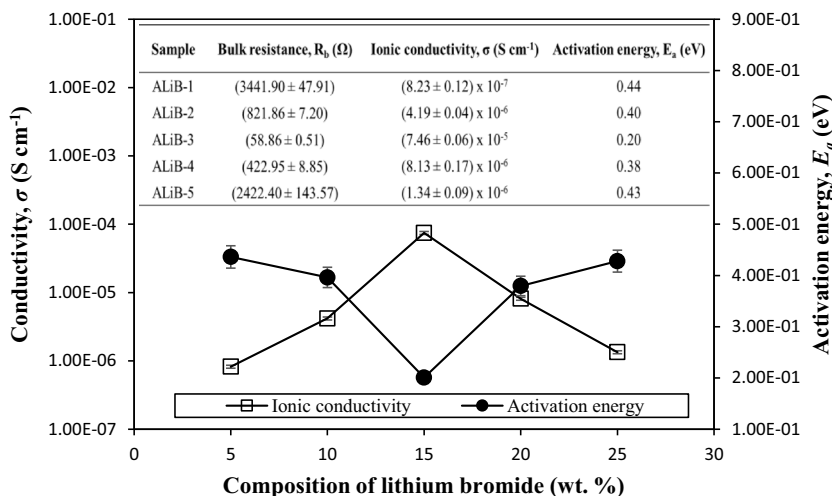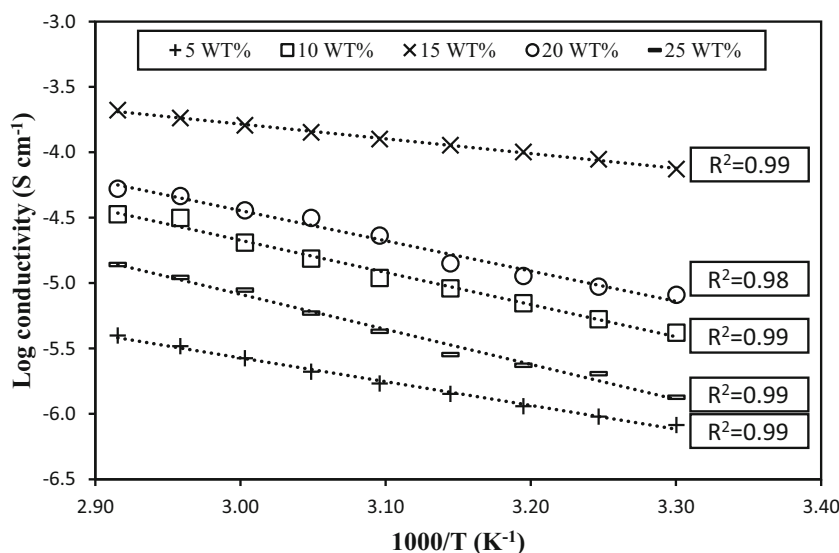

Sample	Bulk resistance, R_b (Ω)	Ionic conductivity, σ (S cm^{-1})	Activation energy, E_a (eV)
ALiB-1	(3441.90 ± 47.91)	$(8.23 \pm 0.12) \times 10^{-7}$	0.44
ALiB-2	(821.86 ± 7.20)	$(4.19 \pm 0.04) \times 10^{-6}$	0.40
ALiB-3	(58.86 ± 0.51)	$(7.46 \pm 0.06) \times 10^{-5}$	0.20
ALiB-4	(422.95 ± 8.85)	$(8.13 \pm 0.17) \times 10^{-6}$	0.38
ALiB-5	(2422.40 ± 143.57)	$(1.34 \pm 0.09) \times 10^{-6}$	0.43

Fig. 10 Ionic conductivity of alginate-LiBr SBEs system at different temperature

range from 303 to 343 K. The temperature assists the enhancement of the ionic conductivity in SBEs system. The increment in temperature boosts the kinetic energy of molecules in polymer to eliminate the weak interactive bonds between oxygen atoms of alginate, and Li cations [81]. Due to the increment of thermal stability (refer to TGA analysis), Li^+ ions are more easily decoupled from polymer backbone, which assists the ionic migration with the polymer matrix, which in turn increases the ionic conductivity at elevated temperature. The temperature-dependent study of the SBEs system obeys the Arrhenius characteristics, where the regression value, R^2, is in the range of 0.95 to 0.99 [82]. Therefore, the mechanism of cation transport can be associated with that of what transpired in ionic crystals where ions jump to the nearest vacant sites, causing the DC ionic conductivity to increase to a higher value [83]. It is noteworthy to mention that at high temperature, the energy would be large enough to overcome the potential barriers that is created between the sites and thus leads to the increase in the free volume of the system, which in turn facilitates the segmental motion of ionic charge carriers [84]. In order to probe the ion dynamics of SBEs system, the activation energy of electrical conduction (E_a) for the SBEs system has been calculated from the slope of the linear fitting based on Arrhenius relationships [85]:

$$\sigma = \sigma_o \exp\left(-\frac{E_a}{kT}\right) \qquad (6)$$

where σ_o is a pre-exponential factor, k is the Boltzmann constant, and T is the temperature in Kelvin. The E_a is defined as the required energy to overcome the reorganization and reformation of the interactive bonds between polymer chain and Li^+ ions [86]. Figure 9 showed that the E_a reduces as the ionic conductivity increases. The ALiB-3 shown the highest ionic conductivity (7.46×10^{-5} S cm^{-1}) and possesses the lowest

activation energy (0.20 eV). This indicates that lesser energy is required by the charge carriers in higher conducting sample to begin hopping process towards coordinating site of alginate [63].

Transport properties

The transport parameter for SBEs system was determined via FTIR deconvolution technique. Figure 11 depicts FTIR deconvolution of alginate-LiBr in SBEs system. According to Ramlli et al. [87], the area of de-convoluted peak is determined and used if there is a significant change of wavenumber which is believed that the complexation has occurred between the polymer and ionic dopant, suggesting the need of separation between the free ions and contact ions within the region. The region between 1500 and 1800 cm^{-1} was selected due to obvious changes in terms of their band wavenumber as shown from FTIR analysis. Moreover, the previous FTIR analysis depicted a clear absorption peak at 1612 cm^{-1} for ionic dopant due to Li^+ moiety from LiBr. The percentage area of free ions and contact ions of SBEs system were calculated using Eq. 2 and tabulated in Table 2. From Fig. 11, the peak adjacent to ~ 1630 cm^{-1} may be attributed by the free ions, and the peaks adjacent to ~ 1590 cm^{-1} and ~ 1670 cm^{-1}, respectively, can be assigned to the contact ions in the polymer matrix [26, 88, 89]. Table 2 denotes that free ions of SBEs system increased proportionally to LiBr with an addition to up to ALiB-3. This attributes to the increment of ion dissociation from Li^+ to polymer matrix; thus, it directly increases the conductivity value of the SBEs system [90]. Beyond ALiB-3 sample, the percentage of free ions starts to decrease due to re-association of ions, which reduces the ionic conductivity of SBEs system [26, 91].

The numbers of η, μ, and D were calculated using Eqs. 3–5 and were tabulated in Table 2. The μ and D mimic the ionic

Fig. 11 FTIR deconvolution for sample (a) ALiB-1, (b) ALiB-2, (c) ALiB-3, (d) ALiB-4, and (e) ALiB-5 of alginate-LiBr in SBEs system

Electrochemical stability
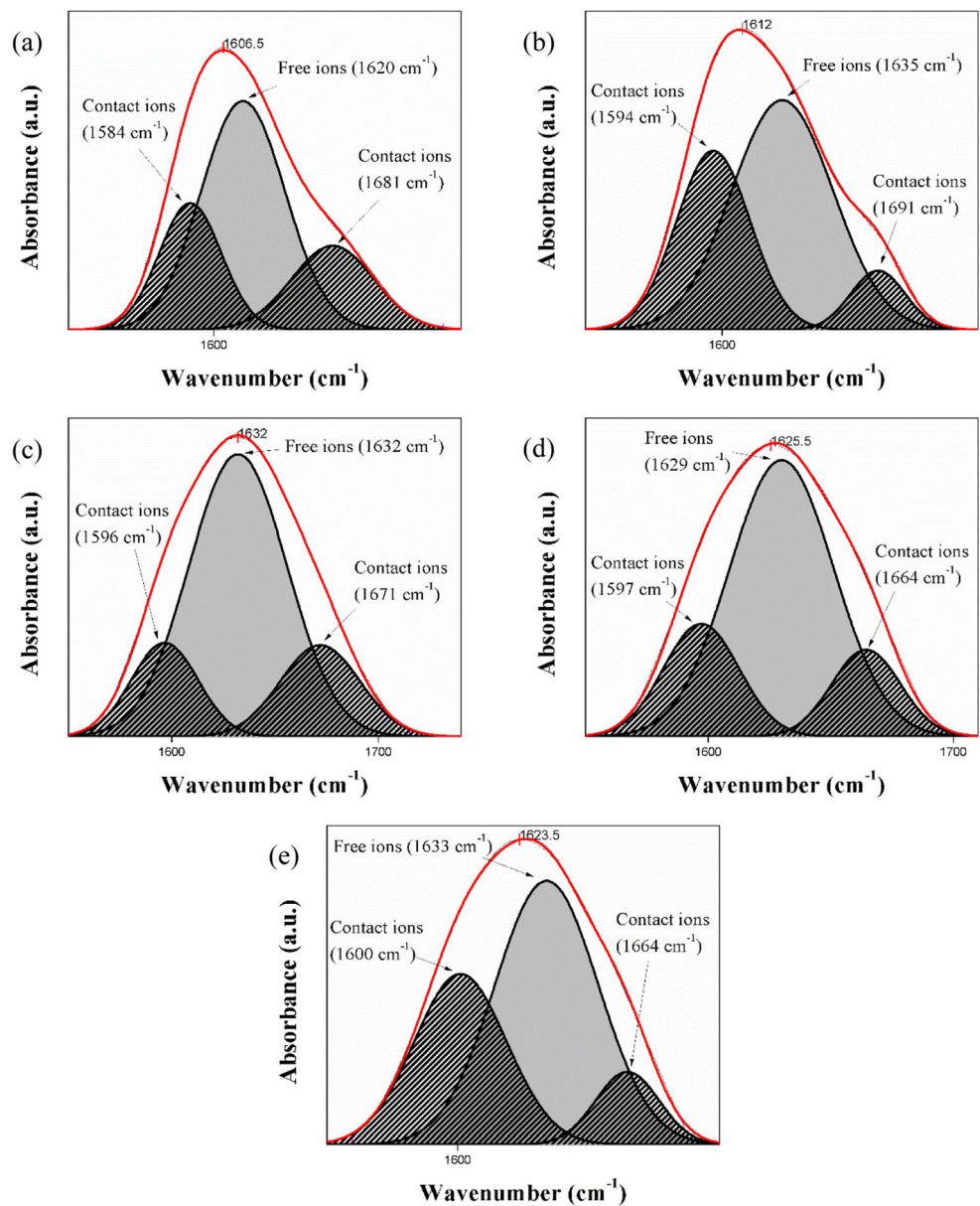
conductivity trend of SBEs system where it achieved optimum value at ALiB-3 and dropped rapidly at ALiB-4. Similar behavior was reported by Arof et al. (2014), where ionic conductivity was governed by the μ and D in their work [69]. The increment of LiBr in SBEs confirmed the assumption made in the FTIR study where the Li^+ from LiBr migrate to lone pair of COO^- from biopolymer matrix. Therefore, the value of μ and D increased which leads to the increment of ionic conductivity and the migration of Li^+ ions only requires lesser activation energy in order to move freely in the backbone of biopolymer [82]. The continuous increment of η above optimum ionic conductivity reflected towards over-crowding of Li^+ ions, and this leads to ion cluster formation, which reduced the ionic conductivity in the SBEs [92].

The LSV is a vital study to determine the working potential of the polymer electrolytes for practical application in electrochemical devices [19, 93]. The electrochemical stability of the SBEs for highest conducting sample (ALiB-3) has been studied using LSV, and the corresponding voltammogram is shown in Fig. 12. There is no significant current that passes through the working SS electrode from the open circuit potential up to 1.25 V, which corresponds to the plating of ALiB-3 sample onto SS electrode, and this may be related to the decomposition of the sample [94]. It increases gradually when the electrode potential is above than 1.25 V. The sample may depend on the processes occurring at the SS electrode [28],

Table 2 Transport parameters of alginate-LiBr in SBEs system

	Contact ions				
Sample	Free ions (%)	Contact ions (%)	η ($\times 10^{22}$ cm^{-2})	μ ($\times 10^{-11}$ cm^2 V^{-1} s^{-1})	D ($\times 10^{-13}$ cm^2 s^{-1})
ALiB-1	56.45	43.55	4.22	12.16	31.75
ALiB-2	58.58	41.42	8.94	30.27	79.01
ALiB-3	67.15	32.85	15.69	296.62	774.21
ALiB-4	66.60	33.40	21.19	23.93	62.48
ALiB-5	57.29	42.71	23.28	3.59	9.39

The free ions and contact ions showed in the table proof that the percentage of ions interact in SBEs system which important to calculation for μ, η, and D.

and the sample working voltage may breakdown at a slightly lower potential under differing conditions. The results showed that 1.80 V is a suitable potential for ALiB-3, and this implies that there is no decomposition of ALiB-3 components at this region. Chitra et al. [95] have reported in their work (i-carrageenan doped with LiClO$_4$) using a similar technique where the working potential breakdown for polymer electrolyte is 2.36 V at room temperature with highest conducting sample value of 3.57×10^{-4} S cm^{-1} and found to be similar with the results obtained in this present work. This finding revealed that the present SBEs system is compatible and has the possibility for application in electrochemical devices since the electrochemical window standard of energy devices is about ~ 1 V [96].

Conclusion

The development of SBEs based on alginate doped with various compositions of LiBr (5–25 wt.%) was successfully prepared via solution casting method. The complexation between alginate and LiBr was investigated by using FTIR analysis which exhibits a significant possible interaction happening at C–O–C stretching, symmetric and asymmetric COO–

stretching. The TGA and DSC analyses depict that SBEs system promoted good thermal stability with the addition of LiBr in the SBEs. It shows that the ionic conductivity values (at ambient temperature) of alginate-LiBr SBEs were found to increase from 4.67×10^{-7} S cm^{-1} for the undoped sample to optimum value at 7.46×10^{-5} S cm^{-1} for sample ALiB-3. The ionic conductivity increment is aligned with the surface morphology and amorphous phase, as revealed by SEM and XRD analyses. The temperature dependence of conductivity for various composition of LiBr follows the Arrhenius characteristics within the studied temperature range. Ionic transport properties based on IR-deconvolution approach have shown that the ionic conductivity of alginate-LiBr SBEs is governed by the μ and D. The LSV revealed ALiB-3 has a possible potential to be used as an electrolyte system for application in electrochemical devices. Further investigation shall be carried out to increase its ionic conduction properties.

Fig. 12 LSV curve for the highest conducting sample (ALiB-3) at 5 mV s^{-1}

References

1. Chen C, Hu L (2018) Nanocellulose toward advanced energy storage devices: structure and electrochemistry. Acc Chem Res 51(12): 3154–3165. https://doi.org/10.1021/acs.accounts.8b00391
2. Zhou B, Zuo C, Xiao Z, Zhou X, He D, Xie X, Xue Z (2018) Self-healing polymer electrolytes formed via dual-networks: a new strategy for flexible lithium metal batteries. Chem Eur J 24(72):19200–19207. https://doi.org/10.1002/chem.201803943
3. Kurapati S, Gunturi SS, Nadella KJ, Erothu H (2019) Novel solid polymer electrolyte based on PMMA: CH$_3$COOLi effect of salt concentration on optical and conductivity studies. Polym Bull:1–19. doi:https://doi.org/10.1007/s00289-018-2659-5
4. Mindemark J, Lacey MJ, Bowden T, Brandell D (2018) Beyond PEO—alternative host materials for Li$^+$-conducting solid polymer electrolytes. Prog Polym Sci 81:114–143. https://doi.org/10.1016/j.progpolymsci.2017.12.004
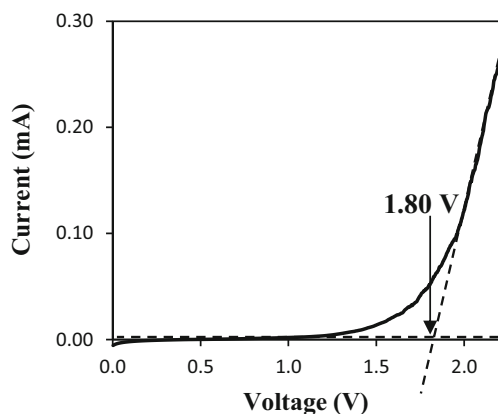
5. Karthika P, Sundaresan B (2018) AC impedance, surface & TGA/DTA analysis of PVC-LiNO₃-CdO. Mech Mater Sci Eng J 14

6. Jia W, Li Z, Wu Z, Wang L, Wu B, Wang Y, Cao Y, Li J (2018) Graphene oxide as a filler to improve the performance of PAN-LiClO₄ flexible solid polymer electrolyte. Solid State Ionics 315:7–13. https://doi.org/10.1016/j.ssi.2017.11.026

7. Singh R, Baghel J, Shukla S, Bhattacharya B, Rhee H-W, Singh PK (2014) Detailed electrical measurements on sago starch biopolymer solid electrolyte. Phase Transit 87(12):1237–1245. https://doi.org/10.1080/01411594.2014.944911

8. Gong S-D, Huang Y, Cao H-J, Lin Y-H, Li Y, Tang S-H, Wang M-S, Li X (2016) A green and environment-friendly gel polymer electrolyte with higher performances based on the natural matrix of lignin. J Power Sources 307:624–633. https://doi.org/10.1016/j.jpowsour.2016.01.030

9. Rani MSA, Rudhziah S, Ahmad A, Mohamed NS (2014) Biopolymer electrolyte based on derivatives of cellulose from kenaf bast fiber. Polym 6(9):2371–2385. https://doi.org/10.3390/polym6092371

10. Yusof YM, Illias HA, Kadir MFZ (2014) Incorporation of NH₄Br in PVA-chitosan blend-based polymer electrolyte and its effect on the conductivity and other electrical properties. Ionics 20(9):1235–1245. https://doi.org/10.1007/s11581-014-1096-1

11. Kadir MFZ, Hamsan MH (2018) Green electrolytes based on dextran-chitosan blend and the effect of NH₄SCN as proton provider on the electrical response studies. Ionics 24(8):2379–2398. https://doi.org/10.1007/s11581-017-2380-7

12. Wang C-S, Virgilio N, Wood-Adams PM, Heuzey M-C (2018) A gelation mechanism for gelatin/polysaccharide aqueous mixtures. Food Hydrocoll 79:462–472. https://doi.org/10.1016/j.foodhyd.2018.01.016

13. Pawlicka A, Firmino A, Vieira D, Sentanin F, Grote JG, Kajzar F Gelatin-and DNA-based ionic conducting membranes for electrochromic devices. In: Optical materials in defence systems technology VI, 2009. International Society for Optics and Photonics, p 74870J. doi:https://doi.org/10.1117/12.835913

14. Ahmad NH, Isa MIN (2015) Structural and ionic conductivity studies of CMC based polymerelectrolyte doped with NH₄Cl. In: Advanced Materials Research. Trans Tech Publ, pp 247–252. doi: https://doi.org/10.4028/www.scientific.net/AMR.1107.247

15. Rahmani V, Sheardown H (2018) Protein-alginate complexes as pH−/ion-sensitive carriers of proteins. Int J Pharm 535(1–2):452–461. https://doi.org/10.1016/j.ijpharm.2017.11.039

16. Ravichandran V, Jayakrishnan A (2018) Synthesis and evaluation of anti-fungal activities of sodium alginate-amphotericin B conjugates. Int J Biol Macromol 108:1101–1109. https://doi.org/10.1016/j.ijbiomac.2017.11.030

17. Lacoste C, El Hage R, Bergeret A, Corn S, Lacroix P (2018) Sodium alginate adhesives as binders in wood fibers/textile waste fibers biocomposites for building insulation. Carbohydr Polym 184:1–8. https://doi.org/10.1016/j.carbpol.2017.12.019

18. Yahya MZA, Arof AK (2004) Conductivity and X-ray photoelectron studies on lithium acetate doped chitosan films. Carbohydr Polym 55(1):95–100. https://doi.org/10.1016/j.carbpol.2003.08.018

19. Monisha S, Mathavan T, Selvasekarapandian S, Benial AMF (2017) Preparation and characterization of cellulose acetate and lithium nitrate for advanced electrochemical devices. Ionics 23(10):2697–2706. https://doi.org/10.1007/s11581-016-1886-8

20. Shukur MF, Ithnin R, Kadir MFZ (2014) Electrical characterization of corn starch-LiOAc electrolytes and application in electrochemical double layer capacitor. Electrochim Acta 136:204–216. https://doi.org/10.1016/j.electacta.2014.05.075

21. Aprilliza M (2017) Characterization and properties of sodium alginate from brown algae used as an ecofriendly superabsorbent. In: IOP Conference Series: Materials Science and Engineering. vol 1.

22. IOP Publishing, p 012019. doi:https://doi.org/10.1088/1757-899X/188/1/012019

22. Zhang N, Xu J, Gao X, Fu X, Zheng D (2017) Factors affecting water resistance of alginate/gellan blend films on paper cups for hot drinks. Carbohydr Polym 156:435–442. https://doi.org/10.1016/j.carbpol.2016.08.101

23. Tong Z, Chen Y, Liu Y, Tong L, Chu J, Xiao K, Zhou Z, Dong W, Chu X (2017) Preparation, characterization and properties of alginate/poly (γ-glutamic acid) composite microparticles. Mar Drugs 15(4):91. https://doi.org/10.3390/md15040091

24. Jiang J-K, Mu Y, Yu H-Q (2019) Differences in the colloid properties of sodium alginate and polysaccharides in extracellular polymeric substances with regard to membrane fouling. J Colloid Interface Sci 535:318–324. https://doi.org/10.1016/j.jcis.2018.10.002

25. Montaser AS, Rehan M, El-Naggar ME (2019) pH-Thermosensitive hydrogel based on polyvinyl alcohol/sodium alginate/N-isopropyl acrylamide composite for treating re-infected wounds. Int J Biol Macromol 124:1016–1024. https://doi.org/10.1016/j.ijbiomac.2018.11.252

26. Rasali NMJ, Nagao Y, Samsudin AS (2018) Enhancement on amorphous phase in solid biopolymer electrolyte based alginate doped NH₄NO₃. Ionics:1–14. doi:https://doi.org/10.1007/s11581-018-2667-3

27. Sabadini RC, Raphael E, Marques ST, Filho PB, Pawlicka A (2014) Alginate-Jeffamine covalently crosslinked hydrogel. Mol Cryst Liq Cryst 603(1):240–247. https://doi.org/10.1080/15421406.2014.967628

28. Sampathkumar L, Selvin PC, Selvasekarapandian S, Perumal P, Chitra R, Muthukrishnan M (2019) Synthesis and characterization of biopolymer electrolyte based on tamarind seed polysaccharide, lithium perchlorate and ethylene carbonate for electrochemical applications. Ionics 25(3):1067–1082. https://doi.org/10.1007/s11581-019-02857-1

29. Mobarak NN, Jumaah FN, Ghani MA, Abdullah MP, Ahmad A (2015) Carboxymethyl carrageenan based biopolymer electrolytes. Electrochim Acta 175:224–231. https://doi.org/10.1016/j.electacta.2015.02.200

30. Che Balian SR, Ahmad A, Mohamed NS (2016) The effect of Lithium iodide to the properties of carboxymethyl κ-carrageenan/carboxymethyl cellulose polymer electrolyte and dye-sensitized solar cell performance. Polym 8 (5). doi:https://doi.org/10.3390/polym8050163

31. Lopes S, Bueno L, Aguiar Júnior FD, Finkler C (2017) Preparation and characterization of alginate and gelatin microcapsules containing Lactobacillus rhamnosus. Anais da Academia Brasileira de Ciências (AHEAD):0-0. Doi:https://doi.org/10.1590/0001-3765201720170071

32. Kadir MFZ, Salleh NS, Hamsan MH, Aspanut Z, Majid NA, Shukur MF (2018) Biopolymeric electrolyte based on glycerolized methyl cellulose with NH₄Br as proton source and potential application in EDLC. Ionics 24(6):1651–1662. https://doi.org/10.1007/s11581-017-2330-4

33. Samsudin AS, Khairul WM, Isa MIN (2012) Characterization on the potential of carboxy methylcellulose for application as proton conducting biopolymer electrolytes. J Non-Cryst Solids 358(8):1104–1112. https://doi.org/10.1016/j.jnoncrysol.2012.02.004

34. Mazuki NF, Fuzlin AF, Saadiah MA, Samsudin AS (2018) An investigation on the abnormal trend of the conductivity properties of CMC/PVA-doped NH₄Cl-based solid biopolymer electrolyte system. Ionics:1–11. doi:https://doi.org/10.1007/s11581-018-2734-9

35. Shukur MF, Hamsan MH, Kadir MFZ (2018) Plasticized and plasticizer free lithium acetate doped polyvinyl alcohol–chitosan blend solid polymer electrolytes: comparative studies. In: Journal of

Physics: Conference Series. vol 1. IOP Publishing, p 012001. doi: https://doi.org/10.1088/1742-6596/1123/1/012001

36. Monisha S, Mathavan T, Selvasekarapandian S, Benial AMF, Aristatil G, Mani N, Premalatha M (2017) Investigation of bio polymer electrolyte based on cellulose acetate-ammonium nitrate for potential use in electrochemical devices. Carbohydr Polym 157: 38–47. https://doi.org/10.1016/j.carbpol.2016.09.026

37. Bakhtin S, Shved E, Bespal'ko Y (2017) Nucleophile-electrophile interactions in the reaction of oxiranes with carboxylic acids in the presence of tertiary amines. J Phys Org Chem 30(12). https://doi.org/10.1002/poc.3717

38. Rasali NMJ, Muzakir SK, Samsudin AS (2017) A study on dielectric properties of the cellulose derivative-NH_4Br-glycerol-based the solid polymer electrolyte system. Makara Journal of Technology 21(2):65–69. https://doi.org/10.7454/mst.v21i2.3082

39. Iwaki YO, Escalona MH, Briones JR, Pawlicka A (2012) Sodium alginate-based ionic conducting membranes. Mol Cryst Liq Cryst 554(1):221–231. https://doi.org/10.1080/15421406.2012.634329

40. Gao C, Pollet E, Avérous L (2017) Properties of glycerol-plasticized alginate films obtained by thermo-mechanical mixing. Food Hydrocoll 63:414–420. https://doi.org/10.1016/j.foodhyd.2016.09.023

41. Zhang Y, Wang C, Liu Y, Jiang W, Han G (2018) Preparation and characterization of composite scaffold of alginate and cellulose nanofiber from ramie. Text Res J:0040517518809041. Doi:https://doi.org/10.1177/0040517518809041

42. Larosa C, Salerno M, de Lima JS, Meri RM, da Silva MF, de Carvalho LB, Converti A (2018) Characterisation of bare and tannase-loaded calcium alginate beads by microscopic, thermogravimetric, FTIR and XRD analyses. Int J Biol Macromol 115:900–906. https://doi.org/10.1016/j.ijbiomac.2018.04.138

43. Choe SR, Haldorai Y, Jang S-C, Rethinasabapathy M, Lee Y-C, Han Y-K, Jun Y-S, Roh C, Huh YS (2018) Fabrication of alginate/humic acid/Fe-aminoclay hydrogel composed of a grafted-network for the efficient removal of strontium ions from aqueous solution. Environ Technol Innov 9:285–293. https://doi.org/10.1016/j.eti.2017.12.008

44. Hodge RM, Edward GH, Simon GP (1996) Water absorption and states of water in semicrystalline poly (vinyl alcohol) films. Polym 37(8):1371–1376. https://doi.org/10.1016/0032-3861(96)81134-7

45. Jinisha B, Anilkumar KM, Manoj M, Pradeep VS, Jayalekshmi S (2017) Development of a novel type of solid polymer electrolyte for solid state lithium battery applications based on lithium enriched poly (ethylene oxide)(PEO)/poly (vinyl pyrrolidone)(PVP) blend polymer. Electrochim Acta 235:210–222. https://doi.org/10.1016/j.electacta.2017.03.118

46. Samsudin AS, Saadiah MA (2018) Ionic conduction study of enhanced amorphous solid bio-polymer electrolytes based carboxymethyl cellulose doped NH_4Br. J Non-Cryst Solids. https://doi.org/10.1016/j.jnoncrysol.2018.05.027

47. Correa E, Moncada ME, Zapata VH (2017) Electrical characterization of an ionic conductivity polymer electrolyte based on polycaprolactone and silver nitrate for medical applications. Mater Lett 205:155–157. https://doi.org/10.1016/j.matlet.2017.06.046

48. Han Y, Yu M, Wang L (2018) Physical and antimicrobial properties of sodium alginate/carboxymethyl cellulose films incorporated with cinnamon essential oil. Food Packag Shelf Life 15:35–42. https://doi.org/10.1016/j.fpsl.2017.11.001

49. Sundaramahalingam K, Muthuvinayagam M, Nallamuthu N, Vanitha D, Vahini M (2019) Investigations on lithium acetate-doped PVA/PVP solid polymer blend electrolytes. Polym Bull:1–26. doi:https://doi.org/10.1007/s00289-018-02670-2

50. Kadir MFZ, Aspanut Z, Yahya R, Arof AK (2011) Chitosan–PEO proton conducting polymer electrolyte membrane doped with NH_4NO_3. Mater Res Innov 15(sup2):s164–s167. https://doi.org/10.1179/143307511X13031890748812

51. Salman YAK, Abdullah OG, Hanna RR, Aziz SB (2018) Conductivity and electrical properties of chitosan-methylcellulose blend biopolymer electrolyte incorporated with lithium tetrafluoroborate. Int J Electrochem Sci 13:3185–3199. https://doi.org/10.20964/2018.04.25

52. Aziz S, Abdullah R, Rasheed M, Ahmed H (2017) Role of ion dissociation on DC conductivity and silver nanoparticle formation in PVA: AgNt based polymer electrolytes: deep insights to ion transport mechanism. Polym 9(8):338. https://doi.org/10.3390/polym9080338

53. Reddy SG, Thakur A (2018) Thermal stability and kinetics of sodium alginate and lignosulphonic acid blends. Iran J Mater Sci Eng 15(3):53–59. https://doi.org/10.22068/ijmse.15.3.53

54. Yang M, Shi J, Xia Y (2018) Effect of SiO_2, PVA and glycerol concentrations on chemical and mechanical properties of alginate-based films. Int J Biol Macromol 107:2686–2694. https://doi.org/10.1016/j.ijbiomac.2017.10.162

55. Rikukawa M, Sanui K (2000) Proton-conducting polymer electrolyte membranes based on hydrocarbon polymers. Prog Polym Sci 25(10):1463–1502. https://doi.org/10.1016/S0079-6700(00)00032-0

56. Liew C-W, Ramesh S (2013) Studies on ionic liquid-based corn starch biopolymer electrolytes coupling with high ionic transport number. Cellul 20(6):3227–3237. https://doi.org/10.1007/s10570-013-0079-0

57. Liu Y, Zhang C-J, Zhao J-C, Guo Y, Zhu P, Wang D-Y (2016) Bio-based barium alginate film: preparation, flame retardancy and thermal degradation behavior. Carbohydr Polym 139:106–114. https://doi.org/10.1016/j.carbpol.2015.12.044

58. Swamy TMM, Ramaraj B, Lee JH (2008) Sodium alginate and its blends with starch: thermal and morphological properties. J Appl Polym Sci 109(6):4075–4081. https://doi.org/10.1002/app.28625

59. Mary IA, Selvanayagam S, Selvasekarapandian S, Srikumar SR, Ponraj T, Moniha V (2019) Lithium ion conducting membrane based on K-carrageenan complexed with lithium bromide and its electrochemical applications. Ionics:1–17. doi:https://doi.org/10.1007/s11581-019-03150-x

60. Huq T, Salmieri S, Khan A, Khan RA, Le Tien C, Riedl B, Fraschini C, Bouchard J, Uribe-Calderon J, Kamal MR (2012) Nanocrystalline cellulose (NCC) reinforced alginate based biodegradable nanocomposite film. Carbohydr Polym 90(4):1757–1763. https://doi.org/10.1016/j.carbpol.2012.07.065

61. Ma X-H, Xu Z-L, Liu Y, Sun D (2010) Preparation and characterization of PFSA–PVA–SiO_2/PVA/PAN difunctional hollow fiber composite membranes. J Membr Sci 360(1–2):315–322. https://doi.org/10.1016/j.memsci.2010.05.031

62. Li X, Xie H, Lin J, Xie W, Ma X (2009) Characterization and biodegradation of chitosan–alginate polyelectrolyte complexes. Polym Degrad Stab 94(1):1–6. https://doi.org/10.1016/j.polymdegradstab.2008.10.017

63. Perumal P, Selvin PC, Selvasekarapandian S (2018) Characterization of biopolymer pectin with lithium chloride and its applications to electrochemical devices. Ionics 24(10):3259–3270. https://doi.org/10.1007/s11581-018-2507-5

64. Nithya S, Selvasekarapandian S, Karthikeyan S, Vinoth Pandi D (2015) Effect of propylene carbonate on the ionic conductivity of polyacrylonitrile-based solid polymer electrolytes. J Appl Polym Sci 132(14). https://doi.org/10.1002/app.41743

65. Kumar LS, Selvin PC, Selvasekarapandian S, Manjuladevi R, Monisha S, Perumal P (2018) Tamarind seed polysaccharide biopolymer membrane for lithium-ion conducting battery. Ionics:1–11. doi:https://doi.org/10.1007/s11581-018-2541-3

66. Unnisa CN, Chitra S, Selvasekarapandian S, Monisha S, Devi GN, Moniha V, Hema M (2018) Development of poly (glycerol suberate) polyester (PGS)–PVA blend polymer electrolytes with NH 4 SCN and its application. Ionics 24(7):1979–1993. https://doi.org/10.1007/s11581-018-2466-x

67. Rezvanian M, Ahmad N, Amin MCIM, Ng S-F (2017) Optimization, characterization, and in vitro assessment of alginate-pectin ionic cross-linked hydrogel film for wound dressing applications. Int J Biol Macromol 97:131–140. https://doi.org/10.1016/j.ijbiomac.2016.12.079

68. Muchakayala R, Song S, Gao S, Wang X, Fan Y (2017) Structure and ion transport in an ethylene carbonate-modified biodegradable gel polymer electrolyte. Polym Test 58:116–125. https://doi.org/10.1016/j.polymertesting.2016.12.014

69. Arof AK, Amirudin S, Yusof SZ, Noor IM (2014) A method based on impedance spectroscopy to determine transport properties of polymer electrolytes. PCCP 16(5):1856–1867. https://doi.org/10.1039/C3CP53830C

70. Arof AK, Noor IM, Buraidah MH, Bandara TMWJ, Careem MA, Albinsson I, Mellander B-E (2017) Polyacrylonitrile gel polymer electrolyte based dye sensitized solar cells for a prototype solar panel. Electrochim Acta 251:223–234. https://doi.org/10.1016/j.electacta.2017.08.129

71. Aziz SB, Abdullah RM (2018) Crystalline and amorphous phase identification from the tanδ relaxation peaks and impedance plots in polymer blend electrolytes based on [CS: AgNt] x: PEO (x-1)(10≤ x≤ 50). Electrochim Acta 285:30–46. https://doi.org/10.1016/j.electacta.2018.07.233

72. Kim D-S, Woo JC, Youk JH, Manuel J, Ahn J-H (2014) Gel polymer electrolytes based on nanofibrous polyacrylonitrile–acrylate for lithium batteries. Mater Res Bull 58:208–212. https://doi.org/10.1016/j.materresbull.2014.01.047

73. Neto MJ, Leones R, Sentanin F, Esperanca JMSS, Medeiros MJ, Pawlicka A, Silva MM (2014) Ionic liquids for solid-state electrolytes and electrosynthesis. J Electroanal Chem 714:63–69. https://doi.org/10.1016/j.jelechem.2013.12.013

74. Chitra R, Sathya P, Selvasekarapandian S, Monisha S, Moniha V, Meyvel S (2018) Synthesis and characterization of iota-carrageenan solid biopolymer electrolytes for electrochemical applications. Ionics 25:1–11. https://doi.org/10.1007/s11581-018-2687-z

75. Shukur MF, Kadir MFZ (2015) Electrical and transport properties of NH4Br-doped cornstarch-based solid biopolymer electrolyte. Ionics 21(1):111–124. https://doi.org/10.1007/s11581-014-1157-5

76. Fuzlin AF, Rasali NMJ (2018) Samsudin AS Effect on ammonium bromide in dielectric behavior based alginate solid biopolymer electrolytes. In: IOP Conference Series: Materials Science and Engineering. vol 1. IOP Publishing, p 012080. doi:https://doi.org/10.1088/1757-899X/342/1/012080

77. Perumal P, Selvin PC, Selvasekarapandian S, Sivaraj P (2019) Structural and electrical properties of bio-polymer pectin with LiClO4 solid electrolytes for lithium ion polymer batteries. Mater Today-Proc 8:196–202. https://doi.org/10.1016/j.matpr.2019.02.100

78. Rasali NMJ (2018) Samsudin AS Characterization on ionic conductivity of solid bio-polymer electrolytes system based alginate doped ammonium nitrate via impedance spectroscopy. In: AIP Conference Proceedings. vol 1. AIP Publishing, p 020224. doi:https://doi.org/10.1063/1.5066865

79. Rani MSA, Ahmad A, Mohamed NS (2018) A comprehensive investigation on electrical characterization and ionic transport properties of cellulose derivative from kenaf fibre-based biopolymer electrolytes. Polym Bull:1–14. doi:https://doi.org/10.1007/s00289-018-2320-3

80. Sonia MML, Anand S, Vinosel VM, Janifer MA, Pauline S, Manikandan A (2018) Effect of lattice strain on structure, morphology and magneto-dielectric properties of spinel NiGdxFe2− xO4 ferrite nano-crystallites synthesized by sol-gel route. J Magn Magn Mater 466:238–251. https://doi.org/10.1016/j.jmmm.2018.07.017

81. Liew C-W, Ramesh S, Ramesh K, Arof AK (2012) Preparation and characterization of lithium ion conducting ionic liquid-based biodegradable corn starch polymer electrolytes. J Solid State Electrochem 16(5):1869–1875. https://doi.org/10.1007/s10008-012-1651-5

82. Salleh NS, Aziz SB, Aspanut Z, Kadir MFZ (2016) Electrical impedance and conduction mechanism analysis of biopolymer electrolytes based on methyl cellulose doped with ammonium iodide. Ionics 22(11):2157–2167. https://doi.org/10.1007/s11581-016-1731-0

83. Othman L, Chew KW, Osman Z (2007) Impedance spectroscopy studies of poly (methyl methacrylate)-lithium salts polymer electrolyte systems. Ionics 13(5):337–342. https://doi.org/10.1007/s11581-007-0120-0

84. Aziz SB, Woo TJ, Kadir MFZ, Ahmed HM (2018) A conceptual review on polymer electrolytes and ion transport models. J Sci Adv Mater Devices 3(1):1–17. https://doi.org/10.1016/j.jsamd.2018.01.002

85. Mazuki NF, Rasali NMJ, Saadiah MA (2018) Samsudin AS Irregularities trend in electrical conductivity of CMC/PVA-NH4Cl based solid biopolymer electrolytes. In: AIP Conference Proceedings. vol 1. AIP Publishing, p 020221. doi:https://doi.org/10.1063/1.5066862

86. Kumar R, Subramania A, Sundaram NTK, Kumar GV, Baskaran I (2007) Effect of MgO nanoparticles on ionic conductivity and electrochemical properties of nanocomposite polymer electrolyte. J Membr Sci 300(1–2):104–110. https://doi.org/10.1016/j.memsci.2007.05.014

87. Ramlli MA, Bashirah NAA (2018) Isa MIN Ionic conductivity and structural analysis of 2-hyroxyethyl cellulose doped with glycolic acid solid biopolymer electrolytes for solid proton battery. In: IOP Conference Series: Materials Science and Engineering. vol 1. IOP Publishing, p 012038. doi:https://doi.org/10.1088/1757-899X/440/1/012038

88. Zainuddin NK, Rasali NMJ, Samsudin AS (2018) Study on the effect of PEG in ionic transport for CMC-NH4Br-based solid polymer electrolyte. Ionics:1–14. doi:https://doi.org/10.1007/s11581-018-2505-7

89. Rasali NMJ, Samsudin AS (2017) Ionic transport properties of protonic conducting solid biopolymer electrolytes based on enhanced carboxymethyl cellulose-NH4Br with glycerol. Ionics:1–12. doi:https://doi.org/10.1007/s11581-017-2318-0

90. Zainuddin NK, Samsudin AS (2018) Investigation on the effect of NH4Br at transport properties in K–carrageenan based biopolymer electrolytes via structural and electrical analysis. Mater Today Commun. https://doi.org/10.1016/j.mtcomm.2018.01.004

91. Chai MN, Isa MIN (2016) Novel proton conducting solid biopolymer electrolytes based on carboxymethyl cellulose doped with oleic acid and plasticized with glycerol. Sci Rep 6:27328. https://doi.org/10.1038/srep27328

92. Ramesh S, Ng KY (2009) Characterization of polymer electrolytes based on high molecular weight PVC and Li_2SO_4. Curr Appl Phys 9(2):329–332. https://doi.org/10.1016/j.cap.2008.03.002

93. Liew C-W, Ramesh S (2015) Electrical, structural, thermal and electrochemical properties of corn starch-based biopolymer electrolytes. Carbohydr Polym 124:222–228. https://doi.org/10.1016/j.carbpol.2015.02.024

94. Samsudin AS, Isa MIN (2015) Conductivity study on plasticized solid bio-electrolytes CMC-NH_4Br and application in solid-state proton batteries. J Teknol 78(6–5). https://doi.org/10.11113/jt.v78.8997

95. Chitra R, Sathya P, Selvasekarapandian S, Meyvel S (2019) Synthesis and characterization of iota-carrageenan biopolymer electrolyte with lithium perchlorate and succinonitrile (plasticizer). Polym Bull:1–25. https://doi.org/10.1007/s00289-019-02822-y

96. Aziz SB, Abdullah RM, Kadir MFZ, Ahmed HM (2018) Non suitability of silver ion conducting polymer electrolytes based on chitosan mediated by barium titanate ($BaTiO_3$) for electrochemical device applications. Electrochim Acta. https://doi.org/10.1016/j.electacta.2018.11.081